ISSN 0036-0236, Russian Journal of Inorganic Chemistry, 2015, Vol. 60, No. 12, pp. 1467–1480. © Pleiades Publishing, Ltd., 2015.
Original Russian Text © N.A. Zakharov, Zh.A. Ezhova, E.M. Koval', A.G. Tkachev, N.T. Kuznetsov, 2015, published in Zhurnal Neorganicheskoi Khimii, 2015, Vol. 60, No. 12, pp. 1606–1620.

SYNTHESIS AND PROPERTIES OF INORGANIC COMPOUNDS

Calcium Hydroxyapatite in Hydroxyapatite/Graphene Oxide/Collagen Nanohybrids

N. A. Zakharov[a], Zh. A. Ezhova[a], E. M. Koval'[a], A. G. Tkachev[b], and N. T. Kuznetsov[a]

[a] *Kurnakov Institute of General and Inorganic Chemistry, Russian Academy of Sciences, Leninskii pr. 31, Moscow, 119991 Russia*

[b] *Tambov State Technical University, Tambov, Russia*

e-mail: zakharov@igic.ras.ru

Received March 12, 2015

Abstract—Interactions between calcium and phosphorus salts, graphene oxide (GO), and collagen (COL) in aqueous solutions have been studied in the $CaCl_2$–$(NH_4)_2HPO_4$–NH_3–H_2O–GO–COL system (25°C) using the solubility (residual concentrations) method and pH measurements. Syntheses were shown to yield composites comprising nanocrystalline calcium hydroxyapatite $Ca_{10}(PO_4)_6(OH)_2$ (HA), GO, and COL of empirical formula $Ca_{10}(PO_4)_6(OH)_2 \cdot x$GO $\cdot y H_2O \cdot z$COL ($x = 0.5$, 1.0, or 2.0; $y = 6.5$–7.7; $z = 3$ or 5 wt %). Some physicochemical characteristics of synthesis products and the effects of the composite formulation on the crystallographic characteristics, sizes, and morphology of nanocrystalline hydroxyapatite (NCHA) were determined and some composition–structure–dispersion–property relationships in the HA/GO/COL composites have been analyzed using chemical analysis, X-ray powder diffraction, IR spectroscopy, thermogravimetry (TGA), differential scanning calorimetry (DSC), and electron microscopy.

DOI: 10.1134/S0036023615120268

A number of nanosized carbon materials that show promise for diversified applications have been prepared in recent years [1]. A special position among these materials is hold by graphene and its derivatives, in particular graphene oxide (GO), which have some unique physical, chemical, and mechanical characteristics [2]. The potential uses of nanosized carbon materials include topical uses associated with their use in electrochemical devices [3, 4], energy storage devices [5, 6], catalysis [7], biosensing [8], drug delivery [9], and materials design for bone implants [10].

Graphene oxide is a carbon allotrope that has a two-dimensional 2D structure and consists of one or more layers of a hexagonal crystal lattice of sp^2 hybridized carbon atoms [11]. Graphene oxide preparation usually involves ultrasonication of graphite oxide [12], which makes GO more commercially accessible than other nanosized carbon materials. This offers a real alternative to carbon nanotubes for use as reinforcing fillers in composites having improved mechanical characteristics. The abundant hydroxy, carboxy, and ethoxy groups on the surfaces and fringes of GO sheets provide a great number of reactive sites for functionalization and interaction with the environment [13]. These features of GO are combined with its exclusive, high mechanical characteristics, a high specific surface area (2600 m^2/g), hydrophilicity, and (according to [9, 14]) biocompatibility and biostability. These specific features of GO allow it to be regarded as an ideal reinforcing material for biocomposites to enhance surface characteristics, interphasial bonds of nanocomposites, and matrix-to-filler stress transfer in the composite [15–18]. These features of GO also stipulated some approaches to solve bone engineering problems directed to the design of functional materials based on graphene and its derivatives comprising biopolymers [19–23] and biologically active inorganic materials [24–27].

Unfortunately, toxicological studies of 2D nanosized carbon materials are now in the initial stage, and any relevant information may be of great value. There is little information about interactions of graphene and its derivatives with biological systems and their toxicity [28]. Available toxicity data imply that, as in other nanosized carbon materials, the specific physicochemical characteristics could play a significant role in the biological activity of the new class of graphene materials [29]. There is evidence for the cytotoxic effect, damaging of plasmatic membrane and mitochondrial activity, generation of oxidative stress, and damaging protein molecules caused by graphene nanomaterials, leading to the neuron death of cells [30–32]. These data are, however, provisional, frequently controversial, and pertain to the properties of graphene-like nanomaterials [14, 33]. The high potential of GO for use in production of composites for medical applications and the growing industrial use of GO [34] make it topical to determine the features of

its interaction with native tissues, in particular, with bone tissue.

Native bone tissue is a natural nanocomposite having a complex hierarchic structure involving several order levels (nano, micro, and macro) [35]. The extracellular matrix of bone tissue is to a considerable extent based on nanosized collagen (COL) fibers (up to 40%) and nanocrystals (~5–50 nm) of bioapatite (nonstoichiometric carbonate-hydroxyapatite) [36], whose crystal-chemical analogues are stoichiometric calcium hydroxyapatite ($Ca_{10}(PO_4)_6(OH)_2$, HA) or its carbonated analogues where CO_3^{2-} ions substitute for OH^- and PO_4^{3-} crystallographic positions [37]. The modeling of bone tissue formation in the course of metabolism in the presence of intentionally introduced nanosized carbon materials (implants) or occasionally involved nanosized carbon materials is a topical task to assess the effect of nanosized carbon materials on HA biomineralization and osteogenesis.

Here, we report on the assessment of the character of interaction of GO with HA (an analogue of the inorganic component of bone tissue) and COL in the course of an in-vitro model experiment to simulate biomineralization in the presence of minor amounts of GO as a contaminant. HA/GO/COL composites were prepared using aqueous solutions of calcium and phosphorus salts in the $CaCl_2$–$(NH_4)_2HPO_4$–NH_3–H_2O–GO–COL (25°C) system, which contained insignificant amounts of GO. The products were characterized by physicochemical methods: chemical analysis, X-ray powder diffraction, IR spectroscopy, thermogravimetry (TGA), differential scanning calorimetry (DSC), scanning (SEM) and transmission (TEM) microscopy.

EXPERIMENTAL

Methods

In the equilibrium liquid phase formed in the reaction of precursors, acidity was measured (I60MI ion meter), Ca^{2+} ions were determined (by complexonometric titration with EDTA solution), and phosphorus was determined as P complexes (by vanadate–molybdate photometric method) [38]. Nitrogen and carbon in the synthesized solids were determined using a Carlo Erba EA 108 NCH analyzer.

X-ray powder diffraction analysis was performed and the crystallographic parameters and crystal sizes of products were determined on a DRON-4 diffractometer (CuK_α, graphite monochromator, EXPRESS control program). Modified full-profile analysis was performed, and Cauchy (D_{hkl}) block size and crystal lattice microstrain were determined using PHAN and PHAN% programs.

The diffuse reflectance IR spectra of products were recorded in the range 4000–400 cm^{-1} on a Nexus (Nicolet) FTIR spectrometer.

The thermal characteristics of the precursor GO were determined under air in the range 20–700°C using TGA and DSC on Universal V4.4A TA Instruments and DSC Q100 V9.8 Build instruments, respectively. The thermal characteristics of products under a helium atmosphere were determined in the range 20–1000°C on a SÒÀ409 thermal analyzer.

The structure and chemical composition of the precursor GO samples were determined using a CamScanS4 electron microscope equipped with a Linc Analytical microanalysis attachment. Microstructure of the precursor GO samples was observed by TEM using a JEOL JEM 1210 microscope.

Syntheses

Hydroxyapatite and HA/GO/COL composite samples were precipitated from aqueous solutions in $CaCl_2$–$(NH_4)_2HPO_4$–NH_3–H_2O (25°C) and $CaCl_2$–$(NH_4)_2HPO_4$–NH_3–H_2O–GO–COL (25°C) systems, respectively. The initial components were aqueous solutions of $CaCl_2$, $(NH_4)_2HPO_4$, and ammonia; aqueous GO slurry; and 2% collagen solution in acetic acid. The aqueous GO slurry for use in the synthesis was prepared from the precursor aqueous GO paste in the course of ultrasonic treatment (0.5 h; frequency: 55 kHz; power: 55 W; instrument: GRAD 13-55).

The synthesis was carried out at constant concentrations of $(NH_4)_2HPO_4$ (0.02 mol/L) and ammonium hydroxide (10 mL conc. aq. ammonia) and constant pH values of 10–10.3 (to inhibit tricalcium phosphate formation). The batch component ratios were: $n_1 = CaCl_2/(NH_4)_2HPO_4 = 1.67$ and $n_2 = GO/(NH_4)_2HPO_4 = 0.083–0.33$. In the synthesis, the $CaCl_2$ solution was added to the aqueous GO slurry and precipitation was carried out by a mixed solution containing $(NH_4)_2HPO_4$ and ammonia. To obtain HA/GO/COL composites containing 3 and 5 wt % COL in the $CaCl_2$–$(NH_4)_2HPO_4$–NH_3–H_2O–GO–COL (25°C) system, the appropriate amount of 2% COL solution in acetic acid was added. The synthesis lasted 14 day in a volume of 200 mL under vigorous magnetic stirring until the aqueous system was completely equilibrated in accordance with the earlier determined [39] conditions for preparing HA and its based composite in $CaCl_2$–$(NH_4)_2HPO_4$–NH_3–H_2O (25°C) systems.

The Ca^{2+} and PO_4^{3-}, contents and molar ratios $n_3 = Ca^{2+}/PO_4^{3-}$ and $n_4 = GO/PO_4^{3-}$ in solid phases were derived from the analysis of residual concentrations in liquid phases after the synthesis reaction was over. The solid phases to be used in analysis were filtered off, washed with distilled water to pH 7, and dried to constant weight under air at room temperature.

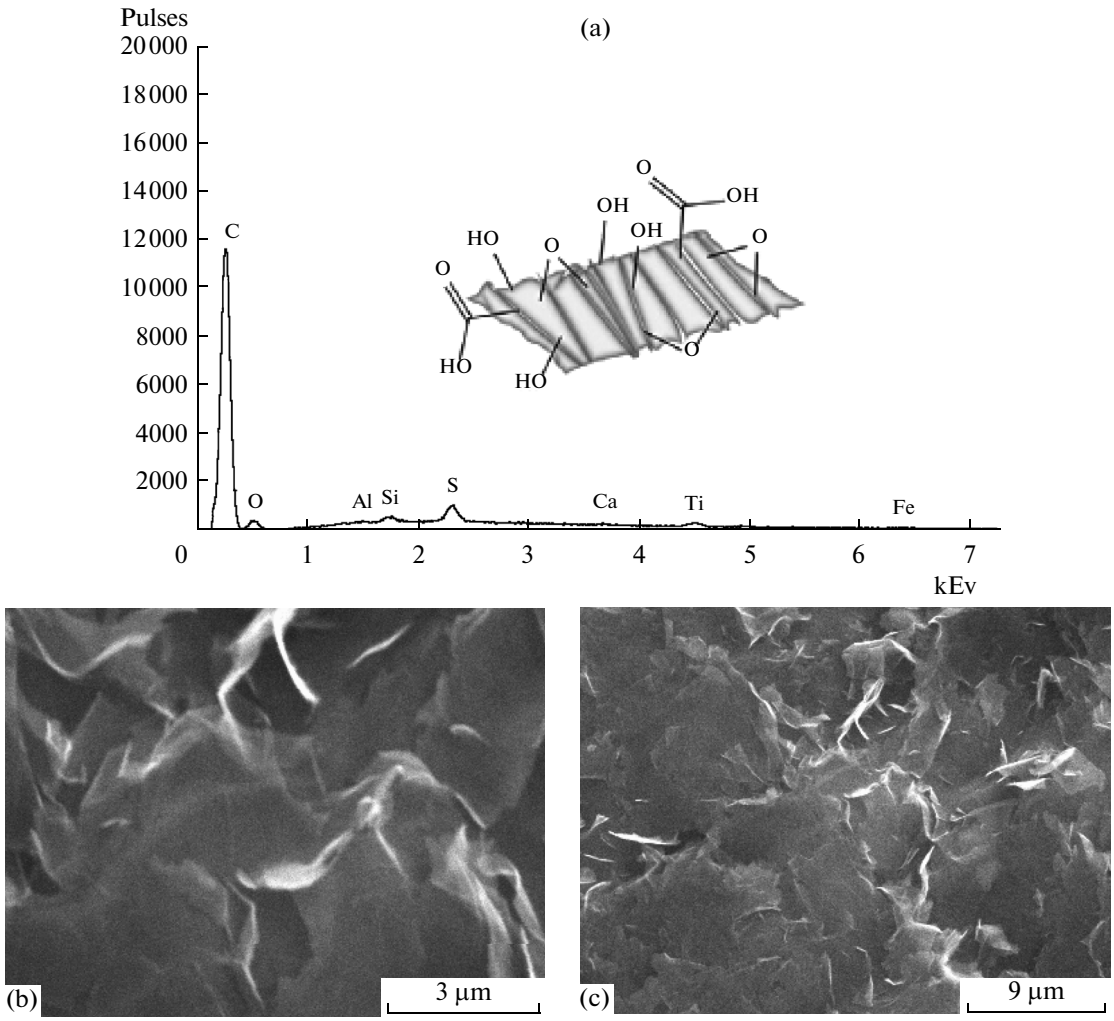

Fig. 1. (a) GO samples used in the synthesis contained ~90 wt % carbon, ~10 wt % oxygen, and Al, Si, S, Ca, Ti, and Fe traces as probed by ESCA. (b, c) SEM images of the GO used in the synthesis at various magnifications.

Physicochemical Identification of the Precursor GO

The GO used to manufacture HA/GO/COL composites was prepared from a natural graphite powder using a modified method described in [40, 41]. The precursor GO contained ~90 wt % carbon and ~10 wt % oxygen as determined by electron spectroscopy for chemical analysis (ESCA) (Fig. 1a). In SEM images, GO layers had a typical appearance of wrinkled sheets (Figs. 1b, 1c).

A low-intensity peak in the region of $2\theta \approx 11°$ of the X-ray diffraction pattern for the precursor GO (Figs. 2a, 2b) indicates an insignificant separation of GO sheets and a low degree of crystallographic order in the GO [41]. The GO diffraction pattern had a certain resemblance to the diffraction characteristics of hexagonal graphite (layer sequence: AB; structure type: A9a; Pearson symbol: *hP*4). The peak in the region $2\theta = 13°$ signifies the presence of amorphous carbon in the precursor carbonaceous material; and the peak in the region of $2\theta = 26°$ is typical of carbon in the form of graphite [42–44]. Reflections from the silica cell constituted the background (Fig. 2a, (*2*)).

The amorphous carbon (Figs. 3a, 3b) present in the precursor GO (Fig. 3c) was identified in the TEM images as individual particles having sizes of ~200 nm, which built up agglomerates ~400 nm in size (Fig. 3a, 3b).

TGA curves for the precursor GO (Fig. 4) indicate that GO decomposition is a multistep process. Water molecules adsorbed on the GO surface vaporize in the temperature range 50–150°C. Decarboxylation starts in the range 150–350°C. At higher temperatures (350–500°C), the hydroxy groups attached to GO sheets are removed. The thermal oxidation of the carbon of GO occurs in the region 550°C.

The IR spectra of the initial aqueous GO slurry GO (Table 1, Fig. 5) feature a broad band from the adsorbate water centered at 3398 cm^{-1} (the stretching of hydroxy groups OH). The vibrations in the region of 1730 cm^{-1} belong to the stretching vibrations of carboxy groups COOH at the fringes of carbon sheets or paired

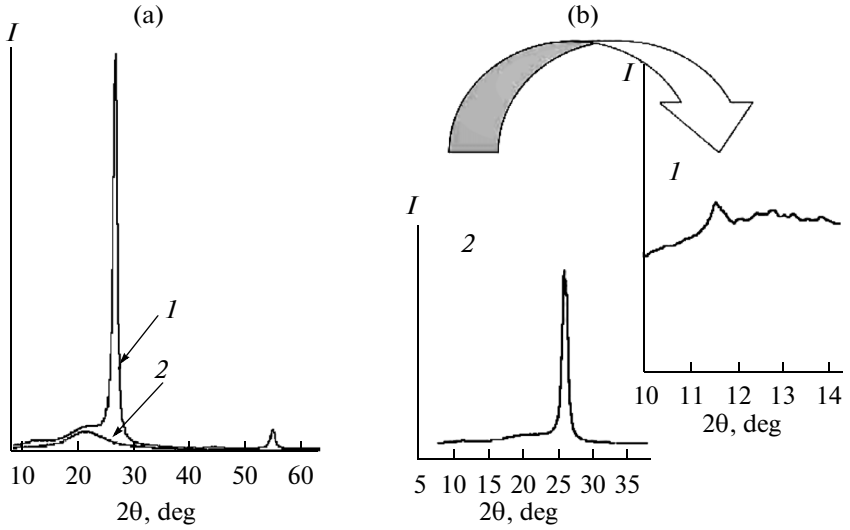

Fig. 2. (a) X-ray diffraction patterns for (*1*) GO and (*2*) background (cell) amorphous silica. (b) (*1*) Enlarged section at small angles of (*2*) the GO diffraction pattern.

carbonyl groups C=O. In the region of 1623 cm^{-1}, there appears a band from the stretching vibrations of C=C. The C–OH stretching vibrations appear as a weak band at 1266 cm^{-1}. The C–O stretching vibrations are identified as a weak band at 1054 cm^{-1}. The surface epoxy groups on carbon sheets are characterized by an absorption band at 833 cm^{-1}.

Composition and Physicochemical Characteristics of Synthesis Products

Chemical analysis of synthesis products. Precipitation from solutions under near-biomimetic conditions yielded either single-phase stoichiometric (Ca/P = 1.67) HA in the $CaCl_2$–$(NH_4)_2HPO_4$–NH_3–H_2O (25°C) system (n_1 = 1.67, pH 10.2 (Table 2) [45]), or stoichiometric HA in the HA/GO/COL composite in the $CaCl_2$–$(NH_4)_2HPO_4$–NH_3–H_2O–GO–COL (25°C) system (Table 2).

The results of physicochemical analysis of reactions between calcium, phosphorus salts and GO in the $CaCl_2$–$(NH_4)_2HPO_4$–NH_3–H_2O (25°C) and $CaCl_2$–$(NH_4)_2HPO_4$–NH_3–H_2O–GO (25°C) systems (Table 2), are based on data gained by chemical analysis of intermediate phases and synthesis products, the determination of phase composition and crystallographic characteristics by X-ray diffraction methods, and thermoanalytical data.

These results (Table 2) imply that the composition of the synthesis products is primarily determined by the ratio Ca/P in the reacting precursors. The base of the resulting composites is stoichiometric HA (Ca/P = 1.67). A change in GO content had almost no effect on the composition of calcium phosphate products (HA) that enter the composites, and the GO content of the composite was close to the GO contents in the precursor reaction mixtures.

Solubilities (residual concentrations) signify that, regardless of GO concentration in the precursor mixtures, the equilibrium liquid phases after the reaction is over contain only insignificant amounts of Ca^{2+} = 0.0002 g-ion/L and PO_4^{3-} = 0.00012 g-ion/L (Table 2). The synthesis conditions (n_1 = 1.67, pH 10–10.3, stirring time: 14 days) were such that provided a virtually complete transfer of Ca^{2+} and PO_4^{3-} to solids as a result of the reaction of $CaCl_2$ with $(NH_4)_2HPO_4$. The ratios Ca^{2+}/PO_4^{3-} in solid phases derived from the analyses of equilibrium liquid phases were 1.67, which indicates that stoichiometric HA in HA/GO/COL composites is formed in all synthesis products.

Table 1. Vibration types and frequencies of GO functionalities

Vibrations	OH	C=O COOH	C=C	C–OH	C–O	C–O–C
Vibration frequencies, cm^{-1}	3398	1730	1623	1348	1054	833

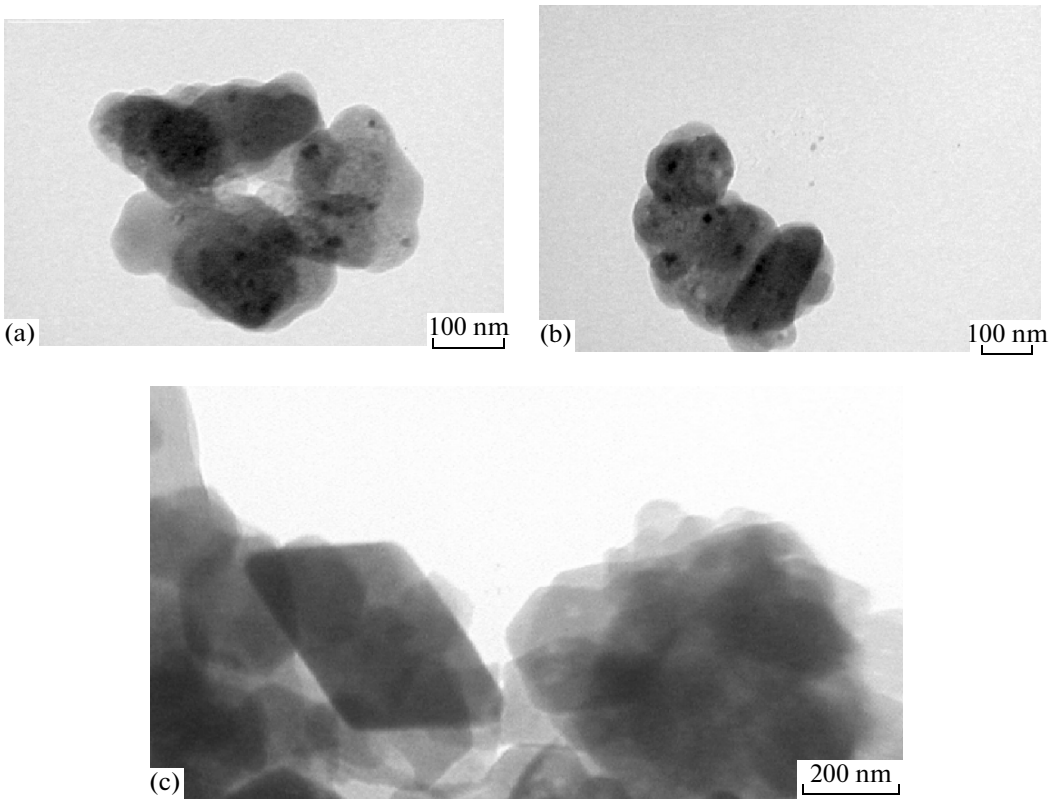

Fig. 3. (a, b) Amorphous carbon particles in the precursor GO and (c) GO sheets as shown by TEM.

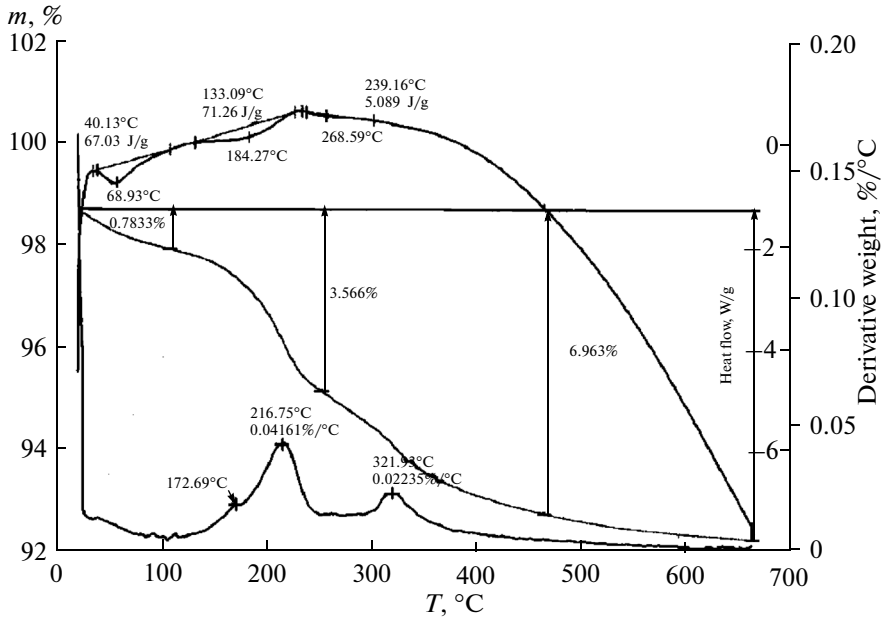

Fig. 4. TGA and DSC curves for the initial GO.

After settling and precipitation of a solid (synthesis products), the liquid phase became clear, and the precipitate color varied, depending on the GO content in the HA/GO/COL composite, from light gray (Table 2; runs 2, 5) to black tints (Table 2; runs 4, 7).

The results of chemical analysis and instrumental NCH analysis (Table 3) indicate the complete transfer of GO to solid synthesis products (Table 2; runs 2–7). The products formed after precipitation were homogeneous composites containing NCHA, GO, and

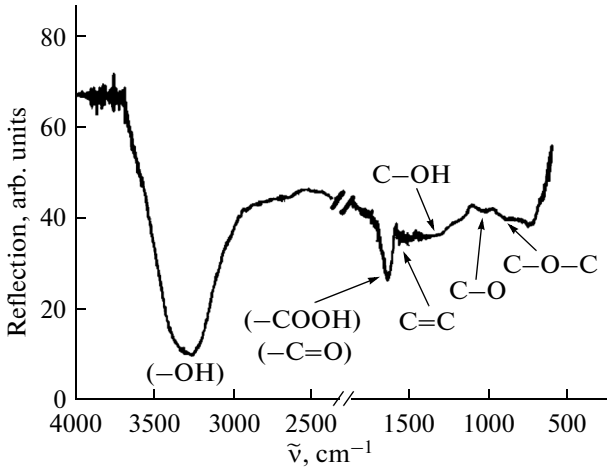

Fig. 5. IR reflection spectra for the precursor GO (aqueous slurry).

COL with the empirical formula $Ca_{10}(PO_4)_6(OH)_2 \cdot xGO \cdot yH_2O \cdot zCOL$ ($x = 0.5$, 1.0, or 2.0; $y = 6.5$–7.7; $z = 3$ or 5 wt %).

X-ray diffraction analysis of synthesis products. The results of X-ray powder diffraction analysis of synthesis products (Table 4) show that hexagonal single-phase stoichiometric (Ca/P = 1.67) NCHA, space group $P6_3/m$, is formed in the $CaCl_2$–$(NH_4)_2HPO_4$–NH_3–H_2O (25°C) system. In the $CaCl_2$–$(NH_4)_2HPO_4$–NH_3–H_2O–GO–COL (25°C) system, hexagonal stoichiometric NCHA is formed in homogeneous $Ca_{10}(PO_4)_6(OH)_2 \cdot xGO \cdot yH_2O \cdot zCOL$ ($x = 0.5$, 1.0, or 2.0; $y = 6.5$–7.7; $z = 3.5$ wt %) HA/GO/COL composites, which contained HA, GO, and COL (Table 2).

X-ray diffraction patterns for heat-untreated HA/GO/COL NCHA composites (Fig. 6, curve *a*) feature poorly pronounced peaks in typical HA reflection regions. To the typical HA reflection region of $2\theta \sim 32°$ (Fig. 6; curves *a*, *b*), there correspond poorly pronounced reflections from planes (211), (300), and (202); they are prominently manifested in annealed (1000°C, 1 h) HA/GO/COL composite samples. The poor resolution and broadening of lines in the X-ray diffraction spectrum of HA in the composites allow us to state that the HA in HA/GO/COL composites has a low degree of crystallinity, just as the crystallinity of HA in bone tissue [46]. At the same time, the X-ray powder diffraction spectra lacked peaks from calcium carbonate ($CaCO_3$), calcium oxide (CaO), and tricalcium phosphate ($Ca_3(PO_4)_2$), which are byproducts frequently encountered in the synthesis of artificial HA [47]. This observation indicates the completion of the reaction in solution under the chosen synthesis conditions for stoichiometric (Ca/P = 1.67) HA. The presence of HA and COL in HA/GO/COL composites had no considerable effect on the diffraction pattern of the HA compared to the diffraction pattern from single-phase stoichiometric HA. The presence of an amorphous COL component in the composite was manifested in the overall spectrum only as the simultaneous vertical shift of all reflections. The effect of GO on the X-ray reflections in HA/GO/COL composites cannot be elucidated, likely because an insignificant GO content in the composite.

The calculated unit cell parameters for HA composites (Table 4) are close to the reference values for stoichiometric HA [48] and for HA samples prepared by other methods [49, 50]. NCHA particles in HA/GO/COL composites are extended along axis *c*

Table 2. Residual concentrations and solids in the $CaCl_2$–$(NH_4)_2HPO_4$–NH_3–H_2O (25°C) and $CaCl_2$–$(NH_4)_2HPO_4$–NH_3–H_2O–GO–COL (25°C)*

Run no.	n_2	c	pH	Found in solution, g-ion/L × 10^3		n_3	n_4	z	In solid phase
				Ca^{2+}	PO_4^{3-}				
System $CaCl_2$–$(NH_4)_2HPO_4$–NH_3–H_2O (25°C)									
1	–	–	10.2	0.3	0.2	1.67	–	–	$Ca_{10}(PO_4)_6(OH)_2 \cdot 6H_2O$
$CaCl_2$–$(NH_4)_2HPO_4$–NH_3–H_2O–GO–COL (25°C)									
2	0.083	1.2	10.2	0.3	0.1	1.67	0.083	3	$Ca_{10}(PO_4)_6(OH)_2 \cdot 0.5GO \cdot 6.7H_2O \cdot zCOL$
3	0.167	1.2	10.2	0.3	0.1	1.67	0.167	3	$Ca_{10}(PO_4)_6(OH)_2 \cdot GO \cdot 7.6H_2O \cdot zCOL$
4	0.33	1.18	10.3	0.3	0.1	1.67	0.33	3	$Ca_{10}(PO_4)_6(OH)_2 \cdot 2GO \cdot 6.8H_2O \cdot zCOL$
5	0.083	2.0	10.2	0.3	0.1	1.67	0.083	5	$Ca_{10}(PO_4)_6(OH)_2 \cdot 0.5GO \cdot 7H_2O \cdot zCOL$
6	0.167	2.0	10.3	0.3	0.1	1.67	0.167	5	$Ca_{10}(PO_4)_6(OH)_2 \cdot GO \cdot 7.2H_2O \cdot zCOL$
7	0.33	2.05	10.2	0.3	0.1	1.67	0.33	5	$Ca_{10}(PO_4)_6(OH)_2 \cdot 2GO \cdot 6.5H_2O \cdot zCOL$

* In batch mixtures: 0.02 mol/L $(NH_4)_2HPO_4$, $n_1 = CaCl_2/(NH_4)_2HPO_4 = 1.67$; $n_2 = GO/(NH_4)_2HPO_4$; c is the amount of 2% COL solution in acetic acid, g. Stirring time: 14 days.

In solids: $n_3 = Ca^{2+}/PO_4^{3-}$, $n_4 = GO/PO_4^{3-}$, and z is COL wt %.

Table 3. Chemical analyses of synthesis products obtained in $CaCl_2$–$(NH_4)_2HPO_4$–NH_3–H_2O (25°C) and $CaCl_2$–$(NH_4)_2HPO_4$–NH_3–H_2O–GO–COL (25°C)*

Synthesis products	Content, wt %						
	Ca	P	OH	H_2O	GO	Collagen (COL)	Weight loss (1000°C)
$Ca_{10}(PO_4)_6(OH)_2 \cdot 6H_2O$	35.91 36.02	16.67 16.72	3.05 3.05	9.97 9.71	–	–	9.97 9.71
$Ca_{10}(PO_4)_6(OH)_2 \cdot 0.5GO \cdot 6.7H_2O \cdot z$COL	34.13 34.12	15.84 15.84	2.90 2.90	10.24 10.27	1.19 1.19	3.0 3.0	14.43 14.46
$Ca_{10}(PO_4)_6(OH)_2 \cdot GO \cdot 7.6H_2O \cdot z$COL	33.25 33.24	15.43 15.43	2.82 2.82	11.33 11.35	2.32 2.32	3.0 3.0	16.65 16.67
$Ca_{10}(PO_4)_6(OH)_2 \cdot 2GO \cdot 6.8H_2O \cdot z$COL	32.84 32.85	15.24 15.25	2.79 2.79	10.08 10.03	4.59 4.59	3.0 3.0	17.67 17.62
$Ca_{10}(PO_4)_6(OH)_2 \cdot 0.5GO \cdot 7H_2O \cdot z$COL	33.27 33.26	15.44 15.44	2.82 2.82	10.44 10.46	1.16 1.16	5.0 5.0	16.60 16.60
$Ca_{10}(PO_4)_6(OH)_2 \cdot GO \cdot 7.2H_2O \cdot z$COL	32.74 32.76	15.19 15.20	2.78 2.78	10.64 10.59	2.29 2.29	5.0 5.0	17.93 17.83
$Ca_{10}(PO_4)_6(OH)_2 \cdot 2GO \cdot 6.5H_2O \cdot z$COL	32.35 32.33	15.01 15.00	2.74 2.74	9.39 9.44	4.52 4.52	5.0 5.0	18.91 18.96

* Numerator: found; denominator: calcd.

Table 4. Crystallographic and morphological characteristics of nanocrystalline stoichiometric HA and NCHA in HA/GO/COL composites

Composite	z, wt %	a, Å	c, Å	Cauchy block size, nm	
				$\parallel c$	$\perp c$
$Ca_{10}(PO_4)_6(OH)_2 \cdot 6H_2O$		9.4274 ± 0.0005	6.8808 ± 0.0002	23.3	12.3
$Ca_{10}(PO_4)_6(OH)_2 \cdot 0.5GO \cdot 6.7H_2O \cdot z$COL	3.0	9.4235 ± 0.0005	6.8762 ± 0.0003	15.5	10.6
$Ca_{10}(PO_4)_6(OH)_2 \cdot GO \cdot 7.6H_2O \cdot z$COL	3.0	9.4231 ± 0.0004	6.8775 ± 0.0003	16.1	10.4
$Ca_{10}(PO_4)_6(OH)_2 \cdot 2GO \cdot 6.8H_2O \cdot z$COL	3.0	9.4287 ± 0.0006	6.8781 ± 0.0003	18.2	11.9
$Ca_{10}(PO_4)_6(OH)_2 \cdot 0.5GO \cdot 7H_2O \cdot z$COL	5.0	9.4270 ± 0.0007	6.8743 ± 0.0004	25.5	14.4
$Ca_{10}(PO_4)_6(OH)_2 \cdot GO \cdot 7.2H_2O \cdot z$COL	5.0	9.4260 ± 0.0004	6.8805 ± 0.0002	19.8	11.9
$Ca_{10}(PO_4)_6(OH)_2 \cdot 2GO \cdot 6.5H_2O \cdot z$COL	5.0	9.4288 ± 0.0006	6.8772 ± 0.0004	13.7	8.8
$Ca_{10}(PO_4)_6(OH)_2 \cdot 2GO \cdot 6.5H_2O$ (1000°C)		9.4195 ± 0.0005	6.8848 ± 0.0005	182.8	
$Ca_{10}(PO_4)_6(OH)_2$		9.418 [48]	6.884 [48]		

and have crystallographic characteristics close to those of NCHA in native bone apatites [51]. The NCHA sizes in the synthesis products were in the range 23.3–13.7 and 12.3–8.8 nm parallel and normal to the hexagonal axis c, respectively. The NCHA size ratio in the prepared composites parallel and normal to the hexagonal axis c varied depending on the composite over rather wide ranges (1.46–1.84).

IR spectroscopy of synthesis products. The IR spectra of synthesis products (Fig. 7) agree with the results of X-ray powder diffraction, indicating the HA formation during the synthesis of HA/GO/COL composites. The characteristic IR bands both in individual HA and in HA in the composite were determined by predominant HA reflections [52] in view of an insignificant content of GO and COL in the composite.

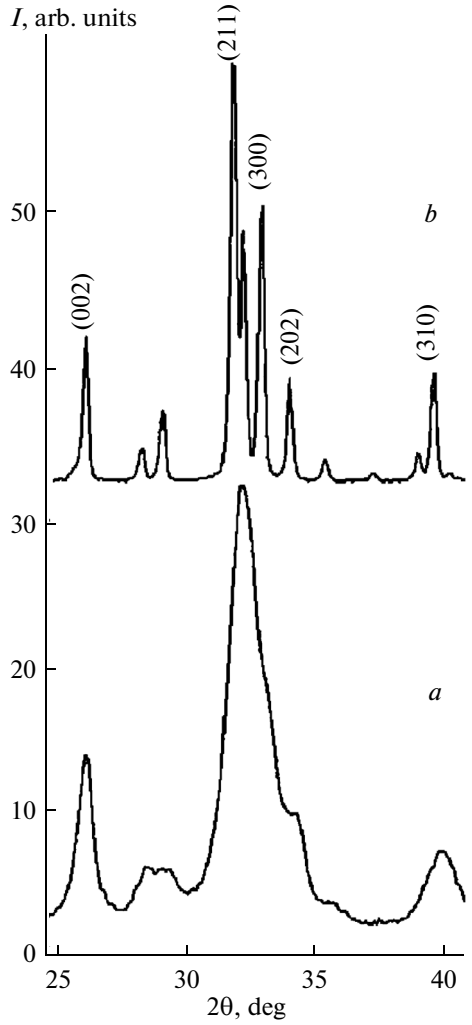

Fig. 6. X-ray diffraction patterns for NCHA in the $Ca_{10}(PO_4)_6(OH)_2 \cdot 2GO \cdot 6.5H_2O \cdot zCOL$ ($z = 5$ wt %) composite (a) before and (b) after annealing (1000°C, 1 h).

The bands associated with the stretching vibrations of phosphate groups PO_4^{3-} were observed in the region of 1092 cm^{-1} (as a poorly pronounced shoulder), at 1037, and at 963 cm^{-1} (Fig. 7). The bending vibrations of PO_4^{3-} groups appeared as bands at 630 and 588 cm^{-1}.

As in native apatite [47, 51] and in some composites of HA and biopolymers [53, 54], the stretching vibrations of OH groups in NCHA at 3570 cm^{-1} had low intensity (Fig. 7). The high sorptive capacity of HA was manifested in IR spectra as a considerable background in the range 3500–2900 cm^{-1} and as a bending vibration band of H–O–H groups at 1671 cm^{-1}.

Products were carbonized in the course of synthesis in air, which is signified by the appearance of bands associated with CO_3^{2-} groups in the IR spectra at 1455, 1422, and 873 cm^{-1}.

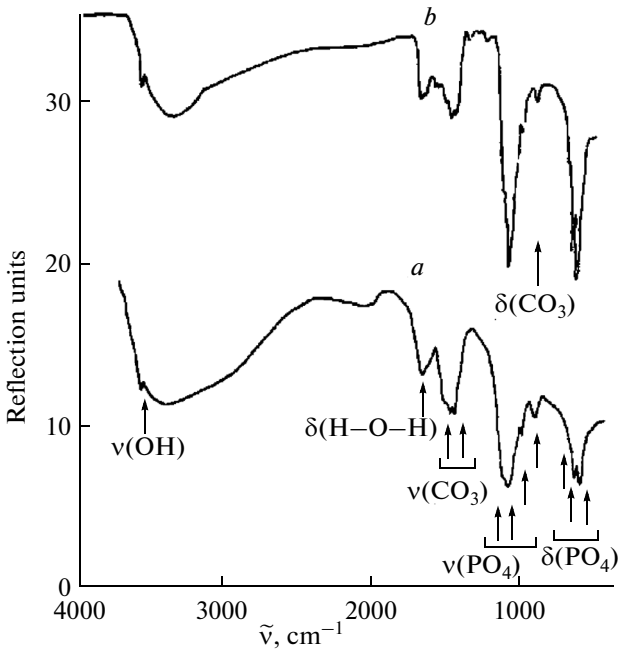

Fig. 7. Diffuse reflectance IR spectra for (a) NCHA and the $Ca_{10}(PO_4)_6(OH)_2 \cdot 2GO \cdot 6.5H_2O \cdot zCOL$ ($z = 5$ wt %) HA/GO/COL composite.

The relative intensities of the main structural units of apatite in the IR spectra of HA/GO/COL composites did not experience significant changes relative to the spectrum of individual NCHA, in spite of the presence of GO and COL (Fig. 7). The COL and GO appeared in the IR spectra as low-intensity bands in the regions 1655–1500 cm^{-1}, which related to the bending vibrations of CO and NH groups in the collagen polypeptide chain [55] and C=C vibrations in the GO at 1623 cm^{-1}.

Thermogravimetric analysis of synthesis products. HA/GO/COL composite samples heated to 1000°C under helium experienced continuous weight loss. The initial weight loss from the $Ca_{10}(PO_4)_6(OH)_2 \cdot 2GO \cdot 6.8H_2O \cdot 3COL$ composites containing 2 wt % GO and 3 wt % COL (Tables 2, 3) in the range 80–100°C, was associated with removal of weakly bonded adsorbate water from the composite (~0.5%) (Fig. 8). An insignificant endotherm in the range 225–275°C corresponds to the degradation and removal of the COL and a further dehydration of the composite. The weight loss of the composite at 275°C was ~4.5%. The endotherm in the range 950–1000°C with an attendant weight loss of ~1% arises from the decarbonization of the composite. The overall weight loss from the exemplary composite upon heating to 1000°C under helium was 12.94%, which agrees with the percentages of the composite components that are degradable under heating.

The product formed upon heating of HA/GO/COL composites to 1000°C, as probed by

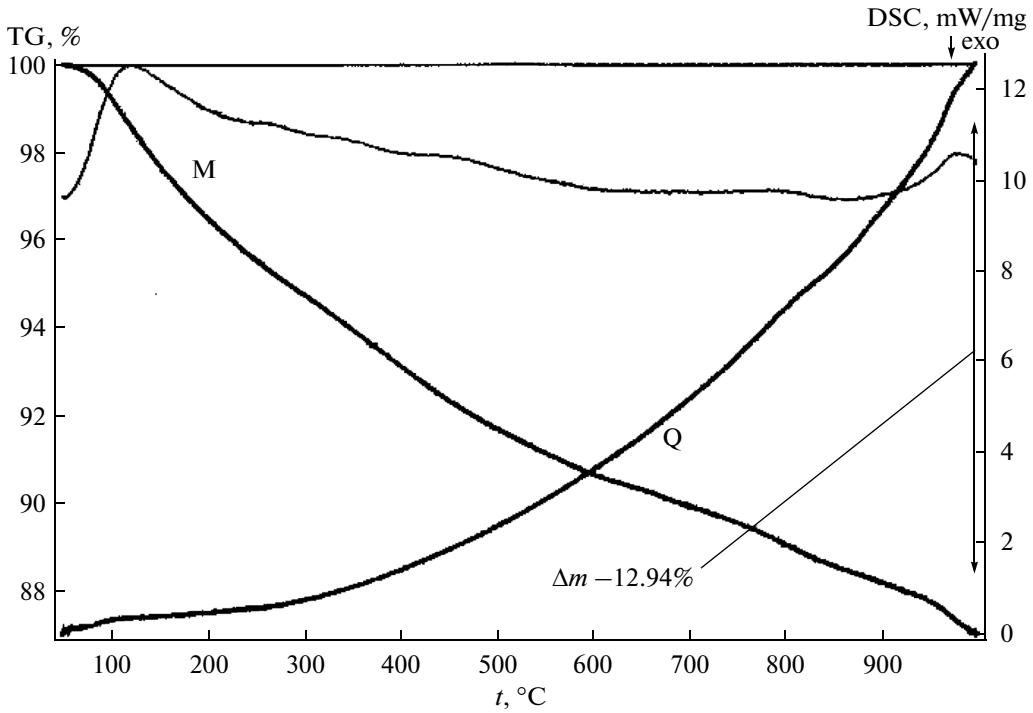

Fig. 8. TGA and DSC curves for the $Ca_{10}(PO_4)_6(OH)_2 \cdot 2GO \cdot 6.8H_2O \cdot zCOL$ ($z = 3$ wt %) HA/GO/COL composite.

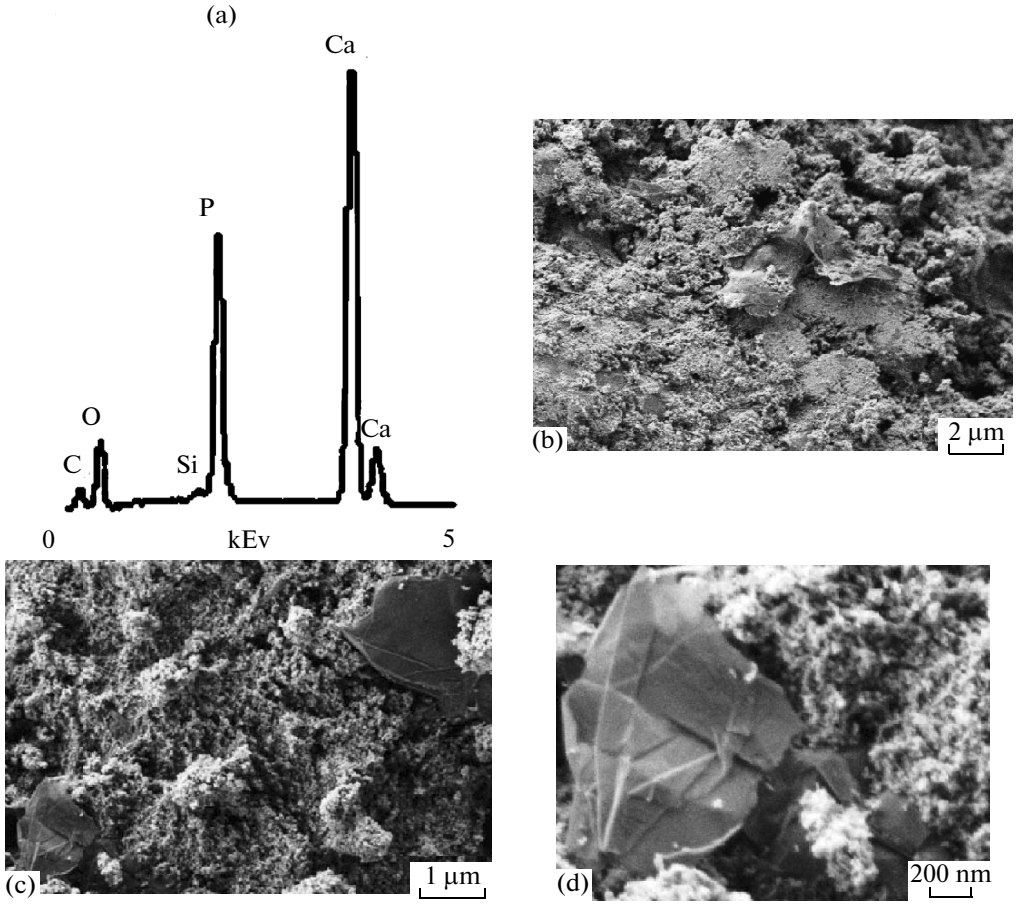

Fig. 9. (a) ESCA analysis and (b, c, d) SEM images for the $Ca_{10}(PO_4)_6(OH)_2 \cdot GO \cdot 7.6H_2O \cdot zCOL$ ($z = 3$ wt %) HA/GO/COL composite.

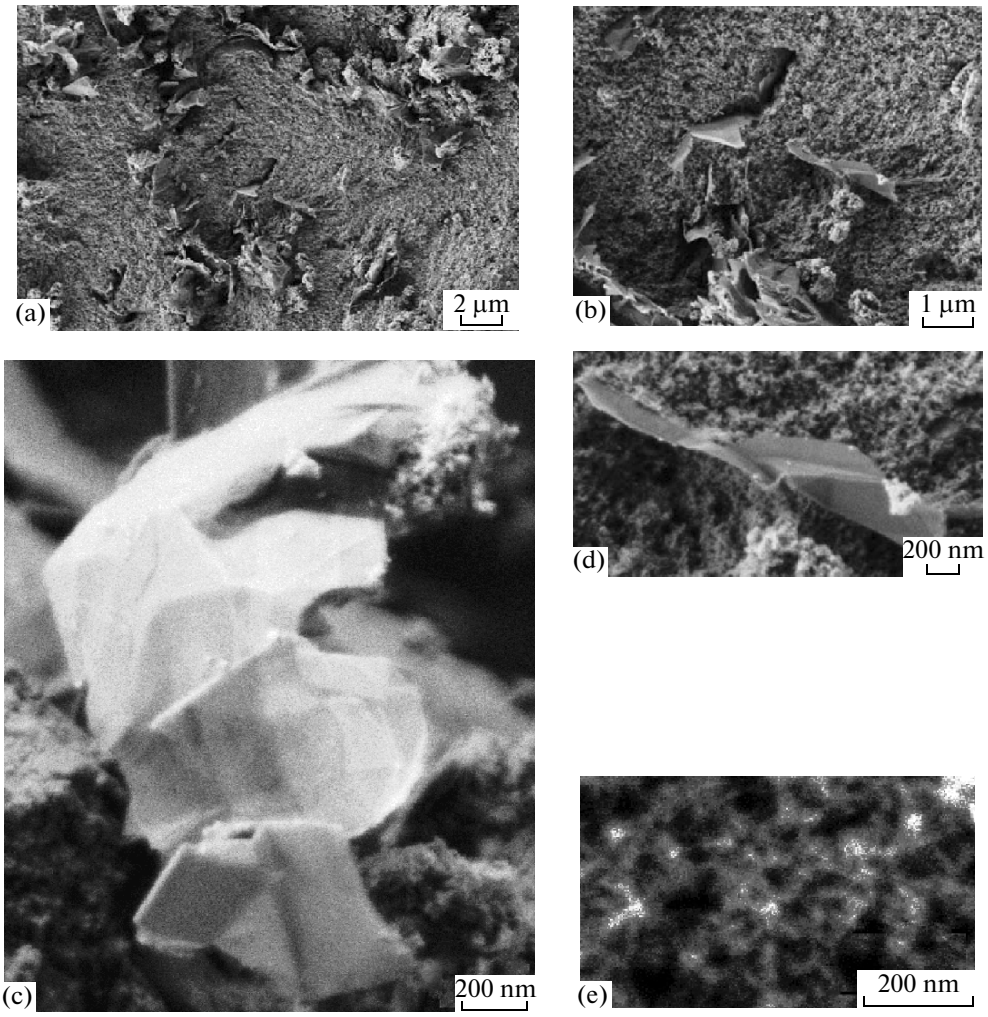

Fig. 10. SEM surface images for the $Ca_{10}(PO_4)_6(OH)_2 \cdot GO \cdot 7.6H_2O \cdot z$COL ($z$ = 5 wt %) HA/GO/COL composite.

X-ray powder diffraction, was stoichiometric (Ca/P = 1.67) HA, whose X-ray characteristics agreed with tabulated values [48] (Table 4). Heat treatment (1000°C, 1 h) produced fine-crystalline HA with grain sizes within ~200 nm (Table 4), as a result of sintering NCHA agglomerates.

SEM morphological analysis of synthesis products. The synthesized HA/GO/COL composites were compositionally uniform. Apart from the major components (Ca, P, O, and C), the composite contained insignificant amounts of silicon (~0.02 wt %) as found by ESCA (Fig. 9a). Graphene oxide was identified in powdered samples of composite synthesis products by the grayish color of the powders.

The SEM images for $Ca_{10}(PO_4)_6(OH)_2 \cdot GO \cdot 7.6H_2O \cdot z$COL composites where z = 3.0 (Fig. 9), and $Ca_{10}(PO_4)_6(OH)_2 \cdot GO \cdot 7.6H_2O \cdot z$COL composites where z = 5.0 (Fig. 10), imply that HA/GO/COL composites consist of spindle-shaped NCHA aggregates having sizes on the order of 100 × 50 nm with GO sheets being incorporated in their mass (Figs. 9b, 9c, 10a, 10b). According to the SEM images (Figs. 9, 10), the GO sheets were randomly arranged over the HA matrix, and there was no any order. In our opinion, the results of SEM did not make it possible to determine the degree of influence of their COL amount (3 or 5 wt %) on the morphological features of the resulting composites.

Graphene oxide sheets yielded to particle surfaces by their planar surfaces (Figs. 9c, 9d, 10c) and by their ends (Figs. 10b, 10e). The GO sheets on the composite surfaces have only separate HA inclusions (Figs. 9d, 10c, 10d) mostly on their fringes (Figs. 9d, 10c) and in kink sites (Fig. 9d).

The hexagonal NCHA with elongated shapes and sizes not exceeding ~26 × 15 nm formed during the synthesis (Table 4), are joint into spindle-shaped aggregates having sizes on the order of 100 × 50 nm, which constitute the major mass of the composite (Figs. 9, 10). One can see from Fig. 10e that interactions of these NCHA agglomerates gives rise to the nanoporous composite structure with pore sizes of ~50 × 100 nm (according to SEM).

RESULTS AND DISCUSSION

The results of physicochemical analysis of the precursor GO and synthesis products brings us to the following conclusions.

(1) The GO used in the experiments was a multilayered nanocarbon material with insignificant defoliation (shown by weak peaks in the region of $2\theta \sim 11°$). Apart from the GO, the carbonaceous material contained minor amorphous carbon (Figs. 3a, 3b) and insignificant amounts of Al, Ti, Si, S, and Fe. Wrinkled GO sheets (Figs. 1b, 1c) contained, as derived from IR spectra, adsorbate water and OH and COOH functional groups, which are reactive with ions in aqueous solutions.

(2) In the course of coprecipitation of calcium and phosphorus salts, GO, and COL from aqueous solutions, either stoichiometric (Ca/P = 1.67) HA was formed in the $CaCl_2$–$(NH_4)_2HPO_4$–NH_3–H_2O (25°C) system or stoichiometric HA in the HA/GO/COL composite was formed in the $CaCl_2$–$(NH_4)_2HPO_4$–NH_3–H_2O–GO–COL (25°C) system. From the determination of residual concentrations (Table 2), we may infer that the reactions in solutions went to completion to form synthesis products as HA or HA in HA/GO/COL composites. The liquid phase after settling was clear and did not contain GO, and the synthesis products changed their color from light gray to saturated gray as their GO content increased. The experimental scheme used is suitable for preparing composites with tailored and controllable compositions, whose empirical formulas may expressed as $Ca_{10}(PO_4)_6(OH)_2 \cdot xGO \cdot yH_2O \cdot z$COL ($x = 0.5$, 1.0, or 2.0; $y = 6.5$–7.7; $z = 3$ or 5 wt %).

(3) The HA produced by the synthesis had crystallographic characteristics similar to tabulated data [48]. Any significant or regular variations in unit cell parameters can hardly be found for hexagonal HA crystals in the composite (Table 4).

However, variations in GO and COL percentages in HA/GO/COL composites can really be traced by the variations in morphology of hexagonal NCHA which are extended along axis *c* (Table 4). For GO-containing composites with 3 wt % COL, increasing GO percentages give rise first to a considerable decrease of crystal lengths along axis *c* relative to individual NCHA, followed by a gradual increase (Fig. 11a). A similar behavior was observed for the HA/GO composites that did not contain COL [56]. For the HA/GO/COL composites containing 5 wt % COL, however, the NCHA length along axis *c* depended on the GO content of the composite in a different manner (Fig. 11b). In this case, NCHA particles were first elongated relative to the individual HA while the GO content in the HA/GO/COL composite was low, and then shortened as the GO amount increased. Thus, when the GO content of the composite was within 1 wt %, NCHA elongation along axis *c* occurred with rising COL content (Figs. 12a, 12b), whereas when the GO content was 2 wt %, the NCHA length decreased with rising COL content (Fig. 12c).

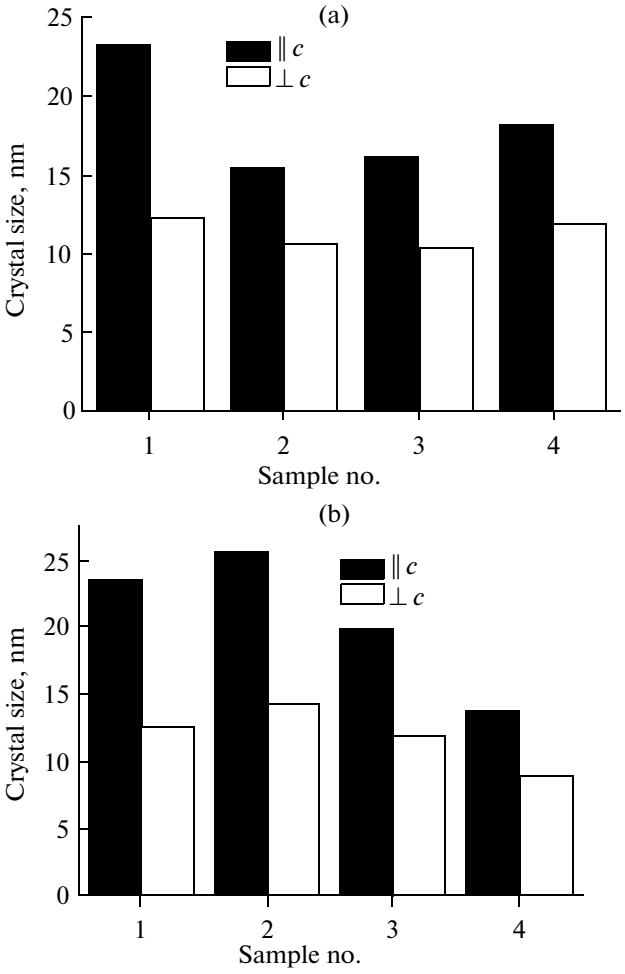

Fig. 11. NCHA sizes for individual HA (sample 1) and HA in HA/GO/COL composites containing (a) 3.0 wt % and (b) 5.0 wt % COL, and 0.5 wt % (sample 2), 1.0 wt % (sample 3), and 2.0 wt % (sample 4) GO.

Our results imply the existence of two competing factors operating in the growth and morphology of NCHA. One factor is nanocarbon GO, which promotes NCHA elongation (Fig. 11a), and the other is biopolymer COL, which results in NCHA shortening as its content in the composite increases (Fig. 11b). Our experimental results yet do not make it possible to characterize the observations to the fullest extent. We may only speak of some threshold values of GO and COL contents in HA/GO/COL composites that give rise to the characteristic alterations in the NCHA morphology and sizes. It seems that the observed crystallization features of NCHA in HA/GO/COL composites are determined by the synthesis method and can differ from the crystallization character of NCHA in the composite under other synthesis conditions. Meanwhile, our results are of interest for the targeted

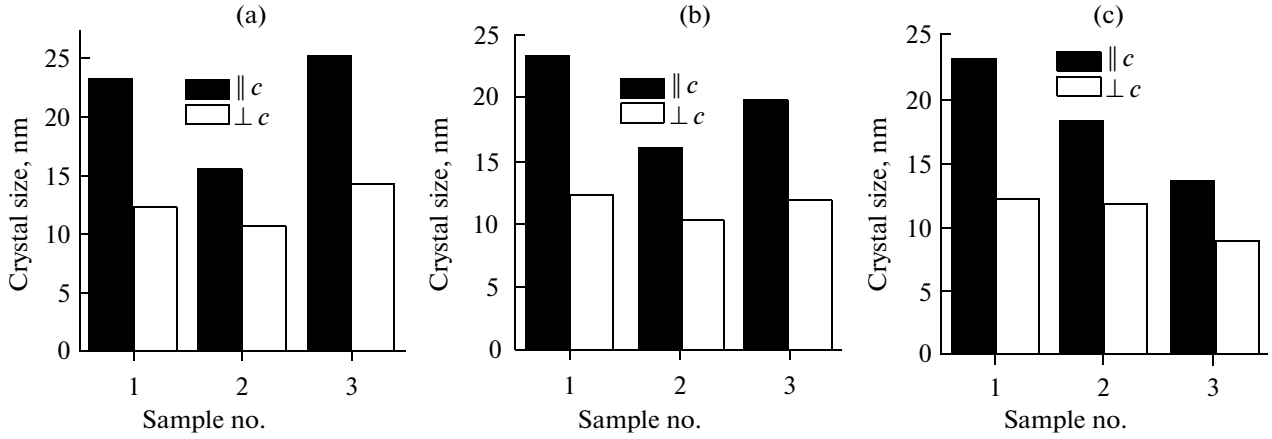

Fig. 12. NCHA sizes for individual HA (sample 1) and HA in HA/GO/COL composites containing (a) 0.5 wt % and (b) 5.0 wt % COL, and 3.0 wt % (sample 2) and 5.0 wt % (sample 3) GO.

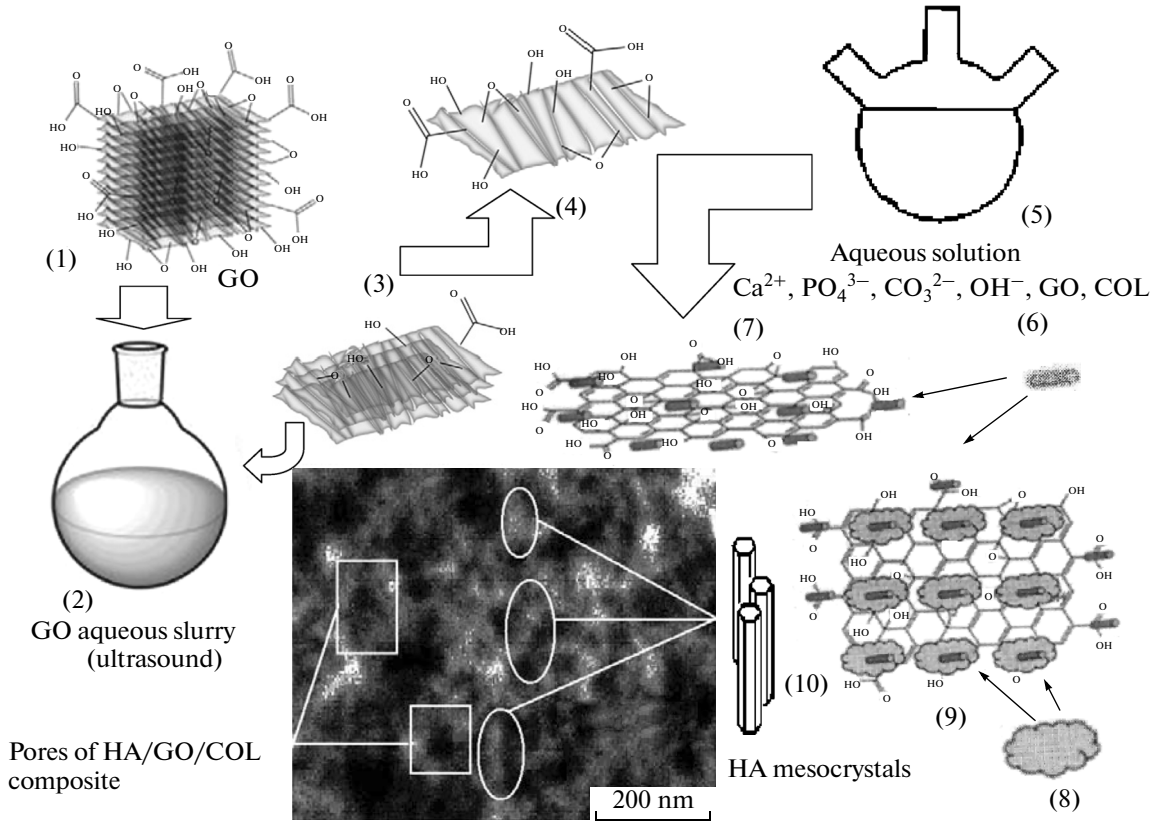

Fig. 13. Graphene oxide (1) and ultrasonic pretreatment of GO slurry(2). GO exfoliation during sonication (3) with characteristic surface functionalities (4). Formation of NCHA during synthesis (5) in solution on the surface of GO layers (7) and COL-functionalized (8) GO layers (9). NCHA intergrowths (10) (mesocrystals) indicated by ellipses on the SEM images and mesopores (rectangles) in HA/GO/COL composite.

synthesis of HA/GO/COL composites with tailored NCHA sizes and morphology.

(4) The apatites formed during the composite synthesis under air contained carbonate ions (Fig. 7), which is also typical of native apatite [37, 46, 47, 51]. The NCHA were agglomerated upon ripening of the precipitate and drying of the synthesis products, to form spindle-shaped druses (Figs. 9, 10) having sizes of ~200 nm. In a similar interaction of hexagonal NCHA and in the presence of an orienting factor (COL), HA mesocrystals can be formed with sizes intermediate between nano- and microcrystals [57–

59]. The HA/GO/COL composite structure arising upon intergrowth of such NCHA entities has a pore structure with pore sizes commensurable to the NCHA inergrowth sizes (Fig. 10, 13).

(5) The above-described route to prepare HA/GO/COL composites to a certain degree models the interactions of calcium and phosphorus salts, COL, and GO in the course of biomineralization during osteogenesis. On the one hand, our results provide some insight into the interaction of GO and bone tissue. On the other, they offer opportunities for the creation of promising and, according to some data [60, 61], biocompatible apatite-based composites for bone implants with synthesis-tailored sizes and morphology of their NCHA.

In summary, we have studied the $CaCl_2$–$(NH_4)_2HPO_4$–NH_3–H_2O–GO–COL (25°C) system using the solubility (residual concentrations) method and pH measurements, and prepared HA/GO/COL composites of empirical formula $Ca_{10}(PO_4)_6(OH)_2 \cdot xGO \cdot yH_2O \cdot z$COL ($x = 0.5$, 1.0, or 2.0; $y = 6.5$–7.7; $z = 3$ or 5 wt %) comprising stoichiometric nanocrystalline HA, GO, and COL. Chemical analysis, X-ray powder diffraction, IR spectroscopy, TGA, DSC, and SEM show that NCHA particles in the thus-prepared HA/GO/COL composites have hexagonal symmetry and comprise carbonate ions. The presence of GO and COL in the course of HA crystallization from solutions has also no effect on the unit cell parameters of NCHA. However, variations in GO and COL contents in HA/GO/COL composites affect the NCHA morphology and sizes and offer an opportunity for the directed synthesis of these composites. The results of in-vitro experiments to a certain degree make it possible to model the effect of GO on the characteristics of native bone NCHA with an intended or occasional involvement of GO in metabolism processes.

ACKNOWLEDGMENTS

This study was in part supported by the Foundations of the Presidium of the RAS and the Chemistry and Materials Science Division of the RAS. Some results of physicochemical analysis were obtained with support of the Shared Facilities Center of the Kurnakov Institute of General and Inorganic Chemistry.

REFERENCES

1. *Springer Handbook of Nanomaterials*, Ed. by R. Vajtai (Springer, Dordrecht/Heidelberg/London/New York, 2012).
2. S. P. Gubin and S. V. Tkachev, *Graphene and Related Carbon Nanospecies* (Knizhnyi Dom, Moscow, 2012) [in Russian].
3. S. J. Park, K. S. Lee, G. Bozoklu, et al., ASC Nano **2**, 572 (2008).
4. D. Y. Cai, K. Yusoh, and M. Song, Nanotecnology **20**, 712 (2009).
5. D. R. Dreyer, S. J. Park, C. W. Bielabski, et al., Chem. Soc. Rev. **39**, 228 (2010).
6. E. R. Margine and M. L. Bocquer, Nano Lett. **8**, 3315 (2008).
7. D. A. Dikin, S. Stankowich, E. J. Zimney, et al., Nature **448**, 6016 (2007).
8. Y. Sun, D. Yu, C. Zeng, et al., Langmuir **26**, 6158 (2010).
9. X. Sun, Z. Liu, K. Welsher, et al., Nano Res. **1**, 203 (2008).
10. M. Li, Q. Lui, Z. Jia, et al., Carbon **67**, 185 (2014).
11. H. P. Boehm, A. Clauss, U. Hofmann, et al., Z. Naturforsch. B-1: Chem. Biochem. Biophys. Biol. Verw. Geb. **17**, 150 (1962)
12. G. Eda and M. Chhowallal, Adv. Mater. **22**, 2392 (2010).
13. D. W. Lee, SantonL. De Los, W. Seo, et al., J. Phys. Chem. B **114**, 5723.
14. Y. Chang, S. T. Yang, and J. H. Liu, Toxicol. Lett. **200**, 201 (2011).
15. H. Tang, G. J. Ehlert, Y. Lin, et al., Nano Lett. **12**, 84 (2012).
16. S. L. Walker, V. R. Marotto, M. A. Rafiee, et al., ACS Nano **5**, 3182(2011).
17. M. A. Rafiee, J. Rafiee, and J. Wang, ACS Nano **3**, 3884 (2009).
18. Y. Li, Q. Peng, and X. He, J. Mater. Chem. **22**, 18748 (2012).
19. X. Wang, H. Bai, Z. Yao, et al., J. Mater. Chem. **20**, 9032 (2010).
20. X. Yang, Y. Tu, L. Li, et al., ACS Appl. Mater. Interfaces **2**, 1707 (2010).
21. H. Fan, L. Wang, K. Zhao, et al., Biomacromolecules **11**, 2345 (2010).
22. J. Pan, T. Wu, H. Bao, et al., Carbohydr. Res. **83**, 1908 (2010).
23. D. Depan, B. Girase, J. Shah, et al., Acta Biomater. **7**, 3432 (2011).
24. S. Kim, S. H. Ku, S. Y. Lim, et al., Adv. Mater. **23**, 2009 (2011).
25. H. Liu, P. Xi, G. Xie, et al., J. Phys. Chem. C **116**, 3334 (2012).
26. L. B. G. Luis, M. Rodrigues-Lorenzo, F. Barroso-Bujans, et al., Key Eng. Mater **396–398**, 477 (2008).
27. A. R. Biris, M. Mahmood, M. Lazar, et al., J. Phys. Chem. **115**, 18967 (2011).
28. V. C. Sanchez, A. Jachak, R. H. Hurt, et al., Chem. Res. Toxicol. **25** (1), 15 (2012).
29. A. Sasidharan, L. S. Panchakarla, P. Chandran, et al., Nanoscale **3**, 2461 (2011).
30. O. Akhavan and E. Ghaderi, ACS Nano **4**, 5731 (2010).
31. Y. Zhang, S. F. Ali, E. Dervishi, et al., ACS Na **4** (6), Ð. 3181 (2010).
32. K.-H. Liao, Y-S. Lin, C. W. Macosko, et al., ACS Appl. Mater. Interfaces **3**, 2607 (2011).
33. Y. Li, Y. Liu, Y. Fu, T. Wei, et al., Biomaterials **33**, 402 (2012).
34. http://patentscope. wipo.int/search/en/result.jsf] (Front page search on “graphene”).

35. M. M. Stevens and G. Mecklenburg, Polym. Int. **61**, 680 (2012).
36. B. S. Kasavina and V. P. Torbenko, *The Life of Bone Tissue* (Nauka, Moscow, 1979) [in Russian].
37. A. M. Smolegovskii, *The History of Phosphate Crystal Chemistry* (Nauka, Moscow, 1986) [in Russian].
38. G. Schwarzenbach and H. Flaschka, *Die komplexometrische Titration* (Ferdinand Enke, Stuttgart, 1965).
39. Zh. A. Ezhova, N. A. Zakharov, E. M. Koval', and V. T. Kalinnikov, Russ. J. Inorg. Chem. **58**, 269 (2013).
40. W. S. Hummers and R. E. Offeman, J. Am. Chem. Soc. **80**, 1339 (1958).
41. N. I. Kovtyukhova, P. J. Ollivier, B. R. Martin, et al., Chem. Mater. **11**, 771 (1999).
42. P. Mahanandia, P. Vishwakarma, K. Nanda, et al., Mater. Res. Bull. **41**, 2311 (2006).
43. V. Labunov, B. Shulitski, A. Prudnikava, and K. Yanushkevich, http://dx.doi.org/10.1088/1742-6596/100/5/052095.
44. W. Li, C. Liang, W. Zhou, et al., J. Phys. Chem. B **107**, 6292 (2004).
45. V. P. Orlovskii, Zh. A. Ezhova, G. V. Rodicheva, et al., Zh. Neorg. Khim. **37**, 881 (1992).
46. J. C. Elliot, *Structure, Chemistry of Apatites and Other Calcium Orthophosphates* (Elsevier, Amsterdam, 1994).
47. L. L. Hench, J. Am. Ceram. Soc. **74**, 1487 (1991).
48. Powder Diffraction File (Inorganic Phases) (JCPDS, ICDD, Newton Square, PA, 1980), No. 9-432.
49. R. Murugan and S. Ramakrishna, Biomaterials **25**, 3829 (2004).
50. V. P. Orlovskii, N. A. Zakharov, S. M. Speranskii, and F. M. Spiridonov, Russ. J. Inorg. Chem. **42**, 1292 (1997).
51. S. V. Dorozhkin, Biomatter **1** (2), 121 (2011).
52. N. A. Chumaevskii, V. P. Orlovskii, Zh. A. Ezhova, et al., Zh. Neorg. Khim. **37**, 1455 (1992).
53. Zh. A. Ezhova and N. A. Zakharov, "Koval' E.M., Kalinnikov V.T," Russ. J. Inorg. Chem. **54**, 477 (2009).
54. N. A. Zakharov, A. E. Chalykh, V. T. Kalinnikov, et al., Kondens. Sredy Mezhfaz. Granitsy **9**, 112 (2007).
55. L. Bellamy, *The Infrared Spectra of Complex Molecules* (London, 1954; Inostrannaya Literatura, Moscow, 1957).
56. Zh. A. Ezhova N. A. Zakharov, E. M. Koval', and V. T. Kalinnikov, Russ. J. Inorg. Chem. **60**, 1 (2015).
57. H. Colfen and M. Antonietti, Angew. Int. Ed. **44**, 5576 (2005).
58. R. Q. Song and H. Colfen, Adv. Mater. **22**, 1310 (2010).
59. J. Fong, B. Ding, and H. Gleiter, Chem. Soc. Rev. **40**, 5347 (2011).
60. M. Li, Q. Lui, Z. Jia, et al., Carbon **67**, 185 (2014).
61. Y. Lui, Z. Dang, Y. Wang, et al., Carbon **67**, 250 (2014).

Translated by O. Fedorova